Letter

Nonreciprocal coupling triggers pinning-depinning transitions of wavefronts in bistable systems chains

L. B. Ramirez-Moya [1,2,*] M. Diaz-Zuniga [2] M. G. Clerc [2] and P. J. Aguilera-Rojas [2]

[1]*Instituto de Ciencias Física y Matemáticas, Facultad de Ciencias, Universidad Austral de Chile, Valdivia, Chile*

[2]*Departamento de Física and Millennium Institute for Research in Optics, FCFM, Universidad de Chile, Casilla 487-3, Santiago, Chile*

(Received 9 January 2025; accepted 12 July 2025; published 1 August 2025)

Coupled discrete systems with reciprocal and nonreciprocal couplings exhibit unexpected and counterintuitive phenomena compared to continuous systems. We investigate the pinning-depinning transition induced by nonreciprocal coupling in nonlinear wave propagation connecting different equilibria in bistable system chains. Theoretically, based on a prototype model of a bistable chain system with nonreciprocal coupling, we show that the latter triggers pinning-depinning transitions of fronts between homogeneous states. Experimentally, we study a chain of bistable systems with nonreciprocal coupling by employing a liquid-crystal light valve with nonreciprocal optical feedback. This system exhibits the propagation of fronts between homogeneous states. The fronts display a pinning-depinning transition by increasing the nonreciprocal coupling, achieved by increasing optical feedback offset. Close to the bifurcation, the front velocity is characterized by a square root law as a function of the bifurcation parameter. We can adequately account for the experimental observations using a tight-binding theoretical model.

DOI: 10.1103/9ypt-4kvs

Introduction. Coupled bistable systems exhibit exciting phenomena, such as the coexistence of extended states, synchronizations, chaos, spatiotemporal chaos, turbulentlike behaviors, domain walls, complex propagation between domains, localized states, and chimera states, among others [1–12]. The spread of domains is usually referred to as fronts. Physical examples of these fronts are nerve impulses along excitable cells [1,2], array of diffusion-coupled flow reactors [3], calcium release waves in cells [4,5], discrete one-dimensional reaction-diffusion systems [6], coupled semiconductor lattices [7], hydrogen-bonded chains [8], and domino waves [9]. In all the above systems, the individual elements are symmetrically coupled to their first neighbors, *reciprocal coupling*. Changing the parameter that characterizes the relative stability of equilibria from a critical value causes fronts to be motionless even though one of the states is more stable. This phenomenon occurs in a range of parameters, called the *pinning range*, and it is known as *failure propagation* [1]. Likewise, failure propagation was initially established in conservative systems [10,11]. The transition from a propagating to a motionless front is known as a pinning-depinning transition introduced in a continuous system [13] and extended to discrete ones [6,12]. The front speed of this transition is characterized by exhibiting a $1/2$ power law as a function of the bifurcation parameter.

Various physical systems have investigated nonreciprocal behaviors in the last few decades due to asymmetric, nonlinear, and non-time-reversal properties. Nonreciprocal responses have been observed in several different systems, including birefringent optical prisms [14], optomechanical resonators [15], asymmetric optical cavities [16], ring-resonant acoustic cavities polarized by a circulating fluid [17], silicon chips [18], magneto-optical photonic crystals [19], optical [20] and mechanical metamaterials [21], and coupled liquid crystals [22]. One of the main effects of nonreciprocal coupling is the generation of an asymmetric propagation of the linear waves and fronts.

This Letter aims to study the pinning-depinning transition of nonlinear waves induced by nonreciprocal coupling. Based on a prototype mathematical model of a bistable chain system with nonreciprocal coupling, we show that the latter coupling triggers pinning-depinning transitions of fronts between homogeneous states. Experimentally, employing a liquid crystal light valve (LCLV) with nonreciprocal optical feedback, we study a chain of optical bistable systems with nonreciprocal coupling. This system exhibits the propagation of fronts between homogeneous states [22]. The fronts exhibit a pinning-depinning transition by increasing the nonreciprocal coupling, achieved by increasing the optical feedback offset. Close to the bifurcation, the front speed is characterized by a square root law as a function of the bifurcation parameter. We can adequately account for the experimental observations using a tight-binding theoretical approach.

Nonreciprocal bistable chain. Let us consider a dimensionless chain of nonreciprocally coupled bistable systems described by

$$\partial_t u_i = \eta + \mu u_i - u_i^3 + (D+\alpha')(u_{i+1}-u_i) + (D-\alpha')(u_{i-1}-u_i), \quad (1)$$

*Contact author: laura.moya.ra@gmail.com

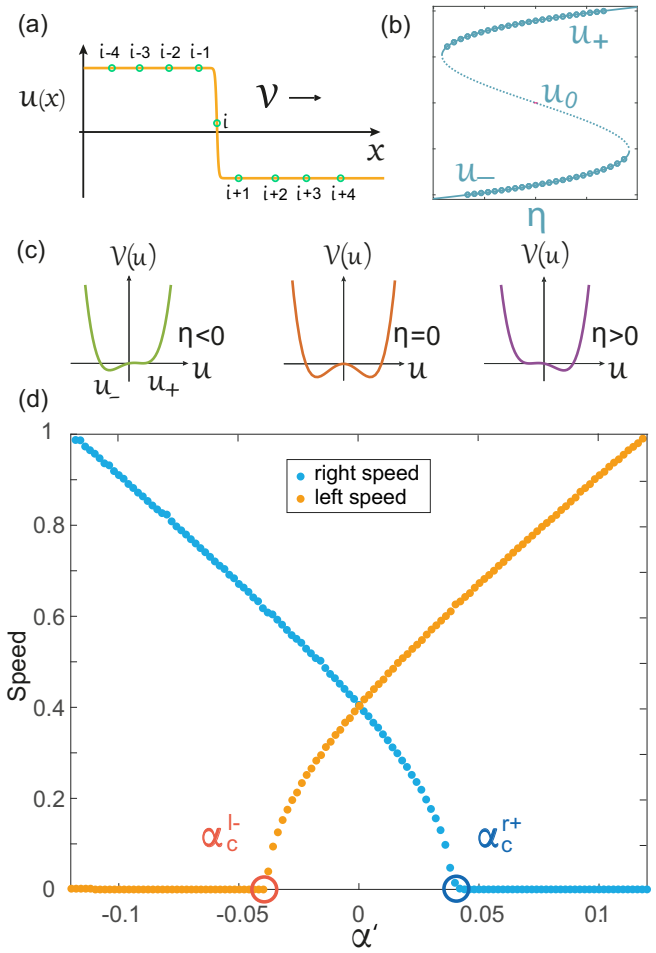

FIG. 1. Pinning-depinning transition of front solution of model Eq. (1) with $\eta = 0.5$, $\mu = 2.2$, and $D = 0.55$. (a) Schematic representation of a front profile. (b) Bifurcation diagram of model Eq. (1) as a function of η. (c) Schematic representation of the local potential $V(u_i)$. (d) Front average velocity as a function of nonreciprocal coupling parameter α'. α_c^{l-} and α_c^{l-} are the critical points of the pinning-depinning transition.

where $u_i(t)$ is an order parameter that accounts for the dynamics of the ith bistable cell. μ and η are the bifurcation parameter and the parameter that control the bistable region, respectively. D and α' are reciprocal and nonreciprocal couplings, respectively. Note that η, μ, D, and α' are dimensionless parameters. The local dynamics, i.e., $D = \alpha' = 0$, of Eq. (1) is potential $\partial_t u_i = -\partial_{u_i} V(u_i)$ with $V(u_i) = -\eta u_i - \mu u_i^2/2 + u_i^4/4$. $V(u_i)$ accounts for a bistable potential (see Fig. 1). The local dynamics has two stable equilibria $u_\pm$ and one unstable u_0.

Equation (1) has propagative solutions (fronts) that asymptotically connect the stable equilibria [12]. Figure 1(a) depicts a front profile. When the nonreciprocal term is zero ($\alpha' = 0$), the system has reciprocal coupling, causing the average velocity front to be the same in both directions, the left and right flanks. However, as the nonreciprocal term increases ($\alpha' > 0$), the front average velocity toward the right flank increases, while the front average velocity toward the left flank decreases. Figure 1(d) illustrates how the front average velocity changes as a function of the nonreciprocal parameter α'. The effect of the nonreciprocal term can be understood in the continuum limit as a drift term responsible for dragging or slowing the front propagation in one or the opposite direction, respectively. Therefore, intuitively, one expects that the nonreciprocal term can induce an absolute convective instability ($\alpha' = \alpha_c^{l-}$ or $\alpha' = \alpha_c^{r+}$); i.e., the front becomes motionless. Since the system is discrete, the front exhibits a motionless region known as the pinning range resulting from the periodical potential induced in the continuous limit [12]. Figure 1(d) shows the pinning range and the pinning-depinning transition points.

In brief, any chain of nonreciprocally coupled bistable systems can exhibit a pinning-depinning transition for fronts when the nonreciprocal coupling is changed. In the following sections, we will study this phenomenon experimentally and explain in more detail the mechanism of pinning-depinning of fronts in discrete systems with nonreciprocal coupling.

Experimental setup. To study the effect of nonreciprocal coupling, we consider an LCLV experiment with nonreciprocal optical feedback illustrated in Fig. 2(a). The LCLV consists of a nematic liquid crystal LC-654 (NIOPIK), which is a mixture of cyano-biphenyls with dielectric anisotropy constant $\epsilon_a = 10.7\epsilon_0$ and large optical birefringence, $\Delta n = 0.2$, placed between two glass layers separated by a distance $d = 15$ μm. Transparent indium tin oxide electrodes and a photoconductive layer are deposed on the glasses to subject the liquid crystal to a driven voltage. A dielectric Bragg mirror with optimized reflectivity for 632.8 nm light is placed in the back layer of the liquid crystal cell. The liquid crystal has planar anchoring in the diagonal direction of the cell for light polarization; that is, the molecules on the cell wall are attached parallel to the cell. The LCLV can be electrically addressed by applying an oscillatory voltage V_0 rms and frequency $f_0 = 1.0$ kHz across the liquid crystal layer. The optical valve is optically forced with a He-Ne laser with a wavelength $\lambda = 632.8$ nm. The LCLV is placed in a $4f$ optical configuration ($f = 25$ cm), as depicted in Fig. 2. The optical feedback circuit is closed with an optical fiber bundle (FB) placed at a distance of $4f$ from the LCLV front face. The optical fiber bundle injects the light into the photoconductive layer, applying an additional voltage to the liquid crystal layer depending on the local light intensity. The system operates in the photoconductor linear regime as a light intensity function. The optical feedback loop is designed so that light simultaneously presents polarization interference induced by the polarizing beam splitter (PBS) and shift of light over a distance α [see Fig. 2(b)]. When there is no displacement ($\alpha = 0$ mm), an illuminated area affects its surroundings isotropically, and when it is displaced, it privileges an area of space. A spatial light modulator (SLM) is considered to carry out different configurations of bistable optical chains.

The SLM allows us to illuminate the optical valve with parallel beams separated by a controllable distance, as illustrated in Fig. 2(a). The experiment is monitored by a complementary metal-oxide-semiconductor (CMOS) camera.

Due to optical feedback, the LCLV exhibits bistability between different molecular reorientations as a function of their applied voltage [23], as illustrated in Fig. 2(c). Namely, for the same parameters, the system exhibits two stable molecular

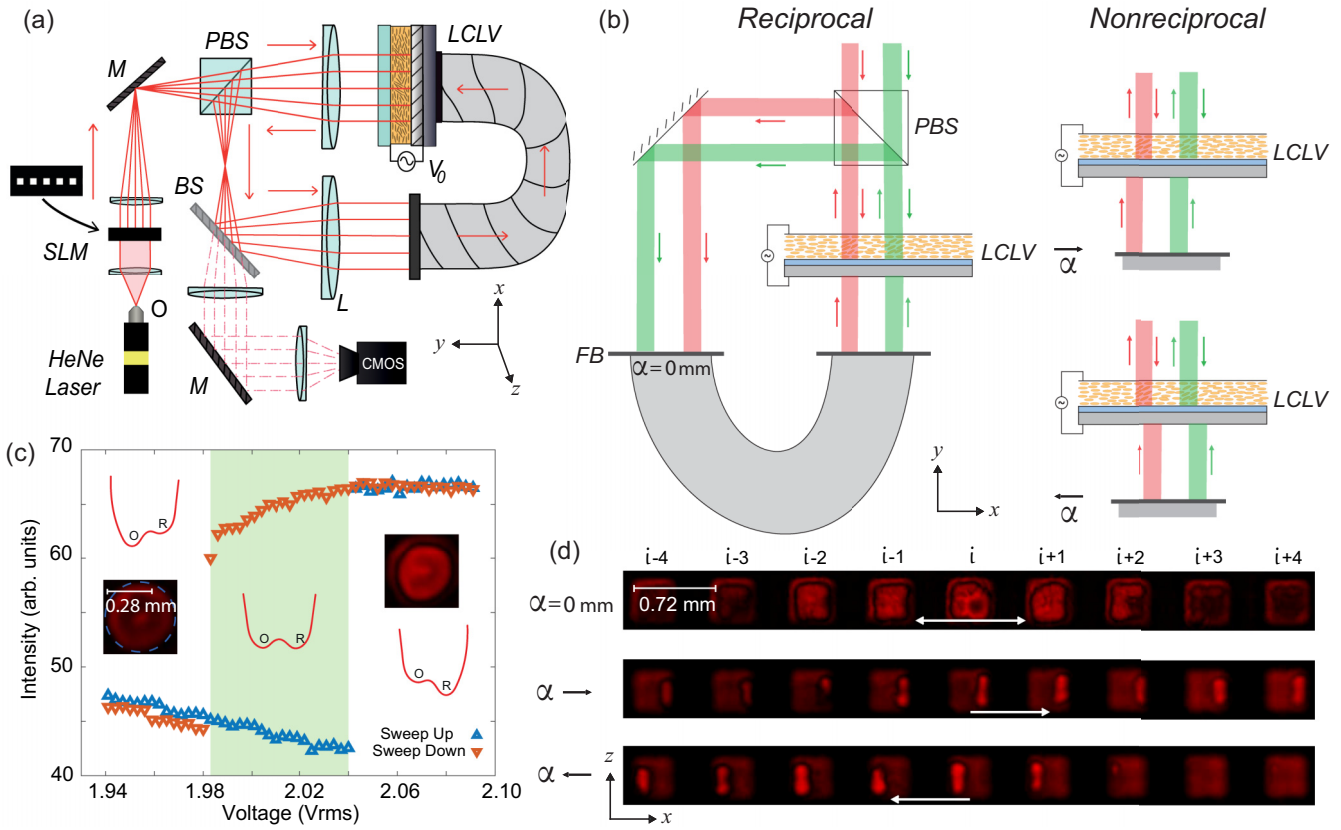

FIG. 2. Liquid crystal light valve with nonreciprocal optical feedback. (a) Schematic representation of an experimental LCLV with nonreciprocal optical feedback. He-Ne laser accounts for a helium-neon laser light source with a wavelength $\lambda = 632.8$ nm. O stands for an optical objective, SLM is a spatial light modulator, M is a mirror, PBS stands for a polarizing beam splitter, V_0 is the intensity of an alternative voltage applied to the LCLV, BS is a beam splitter, L stands for lens, FB is a high-resolution optical fiber bundle, and CMOS stands for a complementary metal-oxide-semiconductor camera. (b) Schematic representation of reciprocal coupling (left panel) and nonreciprocal coupling (right panels). The upper (lower) right panel shows nonreciprocal coupling on the right (left). α accounts for the optical feedback offset. (c) Bifurcation diagram of the LCLV with optical feedback. The intensity of light reflected by the optical valve is a function of the voltage applied to the valve. The up and down triangles account for the light intensity measured by sweeping the voltage up and down, respectively. The painted area (green) accounts for the bistability region. The inset snapshots illustrate the different molecular configurations. The potential schemes show the shape of these in the bistability region. (d) Snapshots of the chain of stable optical systems with reciprocal ($\alpha = 0$ mm) and nonreciprocal ($\alpha \neq 0$ mm) couplings, respectively. The arrows indicate the direction of propagation of fronts.

reorientations, which we can detect by comparing the light emitted by the optical valve. Indeed, one state is brighter and the other is darker. Depending on the initial conditions, this system presents the front propagation between the different equilibria [23]. A spatial light modulator allows us to illuminate the LCLV with parallel beams to generate a bistable system chain. This induces a bistable square cell chain, as illustrated in Fig. 2(a). Figure 2(d) shows the chain of bistable systems with reciprocal and nonreciprocal couplings. By moving the illuminated areas closer or further apart, the reciprocal coupling, generated by the diffusive process associated with the liquid crystal and the voltage induced by optical feedback, can be controlled. Furthermore, the nonreciprocal coupling is controlled by the offset of the optical feedback [cf. Fig. 2(b)].

Nonreciprocal coupling induces pinning-depinning transitions. The system is initially prepared in the dark state, the lower branch of the bifurcation diagram, by decreasing the voltage outside the bistability zone and then moving the voltage toward the bistability region. We consider the voltage where the bright state is more favorable to observe the fronts between the bright state and the dark one. Then, we perturb a central cell by increasing the illumination in this cell thanks to the spatial light modulator, triggering the propagation of the fronts toward both flanks. Figure 3(a) illustrates the typical spatiotemporal evolution of observed fronts. When the coupling is reciprocal ($\alpha = 0$ mm), the front propagation speed toward both flanks is similar [cf. left panel of Fig. 3(a)]. When the optical feedback is moved toward the right flank [$\alpha > 0$; see Fig. 2(b)], the front propagates faster toward the right flank than to the left one, as illustrated in the central panel of Fig. 3(a). Figure 4 summarizes the left and right front speeds as a function of α offset. Intuitively, one expects that as the optical offset increases to the right, the front speed increases toward the right flank and decreases toward the left one [22]. This can be figured out as an *advective effect*. For example, an advective effect is an everyday phenomenon when one tries to swim with or against a flowing river. Counterintuitively, the nonlinear nonreciprocal coupling is responsible for the front speed toward the right flank having a maximum as a function

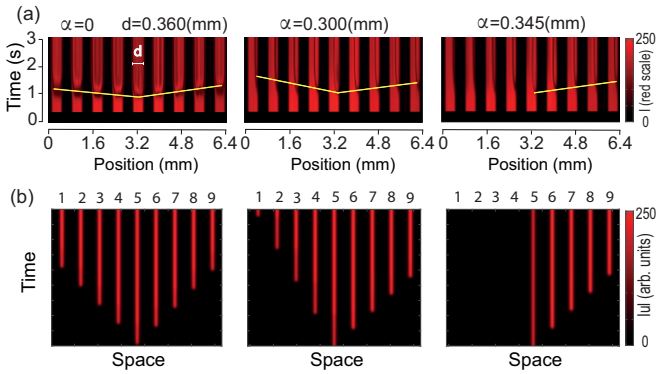

FIG. 3. Experimental (top panels) and numerical (bottom panels) front propagation of the bistable optical chain. (a) The panels illustrate spatiotemporal diagrams where the horizontal axis represents an intermediate spatial line in the bistable optical system chain, and the vertical axis represents the temporal evolution. The colors represent the intensity of the light in arbitrary units. The yellow lines account for the spread of the front. The left, center, and right panels show reciprocal and nonreciprocal couplings shifted to the right flank. (b) Spatiotemporal evolution of numerical front propagation reconstruction of the average molecular reorientation field $\theta(x,t) = \theta_c + \sum_i u_i(t)\Theta(x - x_i)$ using the nonreciprocal bistable chain Eq. (4) with $\eta = 0.5$, $a = 1.0$, $\kappa_- = -1.9 \cdot \alpha'$, $\kappa_+ = 2.1 \cdot \alpha'$, $D = 0.55$, $\mu = 2.2$, $\alpha' = 0$ (left panel), $\alpha' = 0.08$ (middle panel), and $\alpha' = 0.11$ (right panel).

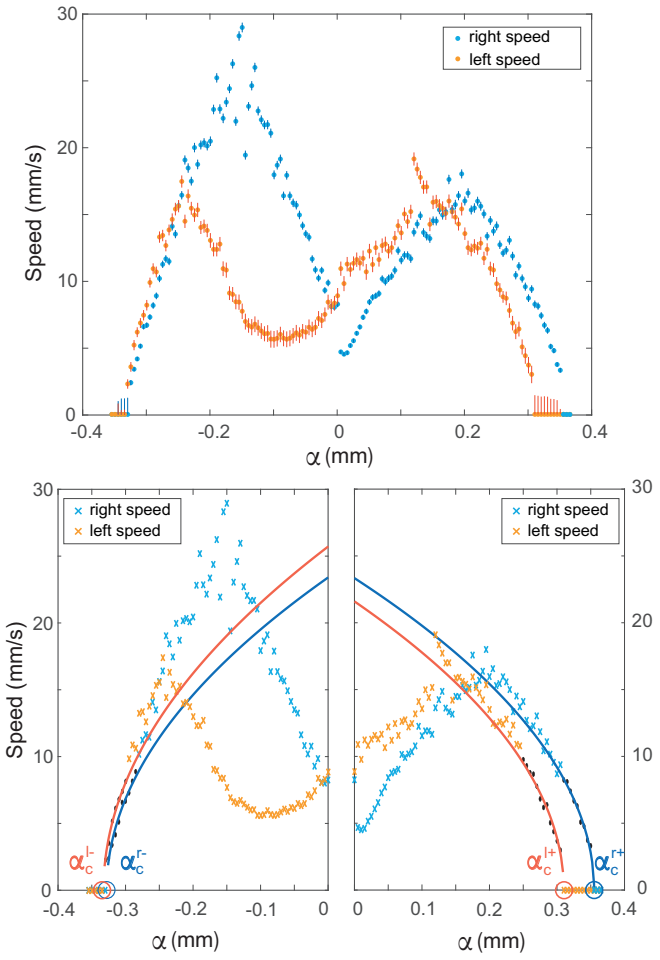

FIG. 4. Front speed as a function of the optical offset. The orange and blue dots indicate the front speed toward the left and right flanks, respectively. The error bars are obtained by determining the front speed for different points in the spatiotemporal diagram. The lower panels show amplifications of the front speed versus the α offset diagram close to the pinning-depinning bifurcations. The continuous curve of the left and right panels is obtained using the fitting $v = \gamma^- \sqrt{|\alpha_c^-| + \alpha}$ ($\alpha < 0$) and $v = \gamma^+ \sqrt{\alpha_c^+ - \alpha}$ ($\alpha > 0$), respectively, where the parameters of the left panel are $\gamma^- = [\gamma^{l-} = 44.63\ \mathrm{mm}^{1/2}/\mathrm{s}, \gamma^{r-} = 40.86\ \mathrm{mm}^{1/2}/\mathrm{s}]$ and $\alpha_c^- = [\alpha_c^{l-} = -0.333\ \mathrm{mm}, \alpha_c^{r-} = -0.328\ \mathrm{mm}]$, and of the right panel are $\gamma^+ = [\gamma^{l+} = 38.80\ \mathrm{mm}^{1/2}/\mathrm{s}, \gamma^{r+} = 39.17\ \mathrm{mm}^{1/2}/\mathrm{s}]$ and $\alpha_c^+ = [\alpha_c^{l+} = 0.310\ \mathrm{mm}, \alpha_c^{r+} = 0.355\ \mathrm{mm}]$. The fitting curves have the following coefficients of determination from left to right: $R^2_{l-} = 0.9920$, $R^2_{r-} = 0.9780$, $R^2_{l+} = 0.9774$, and $R^2_{r+} = 0.9762$.

of the offset α. It is, therefore, expected to find a point at which the front should be motionless. Due to the system's discrete nature, one intuitively expects that the front propagating in the direction opposite to the α offset for a critical value α_c^{l+} will cancel the speed and remain motionless in a parameter range [12]. The right panel of Fig. 4 shows a perturbation in the pinning range; the propagation occurs only in one direction. Close to the pinning-depinning transition point, the front speed v satisfies the kinetic law $v = \gamma\sqrt{\alpha_c^{l+} - \alpha}$, where γ is a dimensional parameter. The bottom panels of Fig. 4 depict this kinetic law. Due to nonlinear reciprocal effects, the front propagating toward the right flank also exhibits a pinning-depinning transition, which presents the same kinetic law as illustrated in Fig. 4. It is important to note that the front velocity versus α offset diagram is not symmetrical concerning this parameter; the primary origin of this asymmetry is the illumination, which is not homogeneous and generates a gradient toward the left flank [22]. We observe the same phenomenon when the optical retro-injection misalignment moves in the opposite direction. However, due to the alignment inhomogeneity, the pinning-depinning transitions for the left- and right-propagating fronts occur in a similar region.

Theoretical description of the bistable optical system with nonreciprocal coupling. The dynamics of the average molecular orientation angle $\theta(x,t)$ of the liquid crystal to the vertical direction of the valve is described by [24]

$$\tau\,\partial_t\theta = l^2\partial_{xx}\theta - \theta + \frac{\pi}{2}\left(1 - \sqrt{\frac{\Gamma V_{\mathrm{FT}}}{\Gamma V_0 + \chi I_w(\theta,\alpha)}}\right), \quad (2)$$

where x and t are the nonreciprocity direction of the liquid crystal layer and time (cf. Fig. 2), respectively. The planar and homeotropic configurations are described by $\theta(x,t) = 0$ and $\theta(x,t) = \pi/2$, respectively. $V_{\mathrm{FT}} \approx 4.5\ V_{\mathrm{rms}}$ is the threshold for the reorientation transition at room temperature (21 °C), $\tau = 100$ ms is the liquid crystal relaxation time, and $l = 30$ μm is the electric coherence length. $I_w[\theta(x+\alpha)] \equiv I_{\mathrm{in}}(x+\alpha)(1 - \cos[\beta\cos^2\theta(x+\alpha)])/2$ is the nonreciprocal optical feedback light intensity reaching at the photoconductor [24], where $I_{\mathrm{in}}(x)$ is the light intensity controlled by the spatial light modulator and $\beta \equiv 2kd\Delta n$, with $d = 15$ μm the thickness of the nematic layer, $\Delta n = 0.2$ the liquid crystal birefringence, and $k = 2\pi/\lambda$ the wavenumber of the light; we employ a

red laser of wavelength $\lambda = 632.8$ nm (He-Ne laser). The effective voltage applied to the liquid crystal layer is $V_{\text{eff}} = \Gamma V_0 + \chi I_w$, $\Gamma = 0.3$ is a transfer factor that depends on the electrical impedances of the photoconductor, dielectric mirror, and liquid crystal, and χ is a phenomenological dimensional parameter that accounts for the linear response of the photoconductor [24].

When the applied voltage V_0 is varied, model Eq. (2) presents several branches of bistability of uniform states resulting from critical values of θ_c. Employing the spatial light modulator close to the Fréedericksz transition, one can induce inhomogeneous illumination, which alternates between a bistable and a monostable region (planar state). Considering that each bistable cell is separated enough, one can use the following ansatz to describe the dynamics of bistable cells (tight-binding-like approach):

$$\theta(x,t) = \theta_c + \sum_i u_i(t)\Theta(x - x_i) + W(x_i, u_i, x), \qquad (3)$$

where $u_i(t)$ is the intensity of the average molecular orientation tilt profile $\Theta(x - x_i)$ in the ith cell, x_i is the middle position of the ith cell, and $W(x_i, u_i, x)$ is the small correction function that accounts for the effects of the other cells at the ith cell. Introducing the previous ansatz into Eq. (2), linearizing in W, and imposing a solvability condition after straightforward calculations, one can obtain

$$\begin{aligned}\partial_t u_i = {} & \eta + \mu u_i - a u_i^3 - (\kappa_+ u_{i+1} - \kappa_- u_{i-1})u_i^2 \\ & + (D + \alpha')(u_{i+1} - u_i) + (D - \alpha')(u_{i-1} - u_i). \qquad (4)\end{aligned}$$

In the Supplemental Material, the relationship between these parameters and the coefficients of Eq. (4) are provided [25].

The model Eq. (4) is an extension of model Eq. (1) with a nonlinear and nonreciprocal coupling. Numerical simulations of Eq. (4) show front propagation between the homogeneous states. Figure 3(b) shows the numerical reconstruction of front propagation in the bistable chain using the ansatz (3) with $\Theta(x - x_i) = \text{sech}^2(x - x_i)$ as the fundamental state function. From these, we observe a behavior quite similar to that observed experimentally; that is, initially, for small nonreciprocity, the speed of the fronts becomes asymmetrical and subsequently decreases. Figure 5 summarizes how the front velocity toward the left and right flanks behaves as a function of the nonreciprocal parameter α'. The behavior of the front velocity as a function of α' is similar to that observed experimentally, where we observe a maximum (see Figs. 4 and 5). Subsequently, the system exhibits two depinning-pinning transition points [see Fig. 5(e)]. Numerically, we observe the same law found experimentally; that is, the velocity satisfies a square root law near the pinning-pinning point.

The transition between the pinning-depinning of fronts and the pinning range phenomenon can be understood as a consequence of the slight energy difference between connected states, which is affected by the system spatial discreteness effects or Peierls-Nabarro potential [12]. In the case of nonreciprocal effects, a new element must be considered to stop the propagation of the front: the advective drift effect, which induces a decrease in the front speed. To understand this, the following two limits can be considered: effective continuous

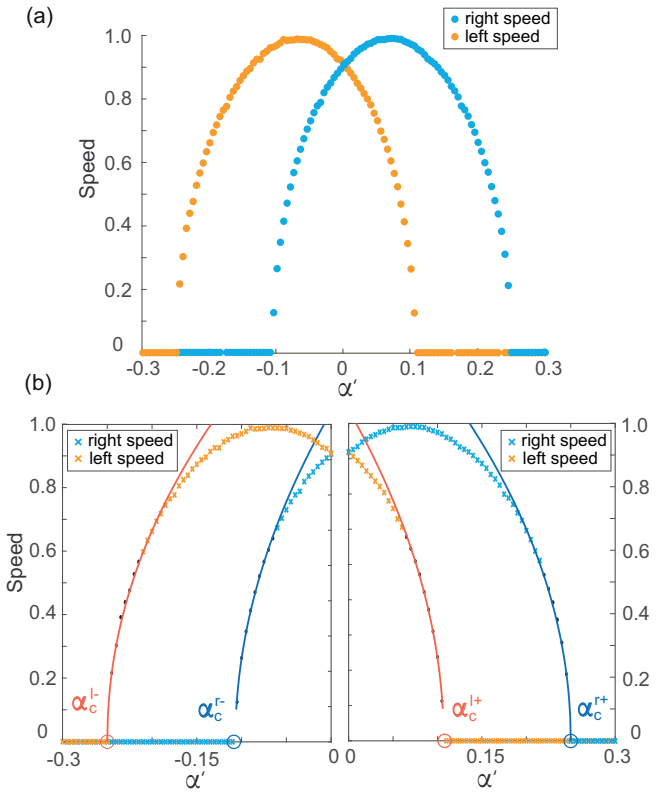

FIG. 5. (a) Front speed propagation of model Eq. (4) with $\eta = 0.5$, $\mu = 2.2$, $a = 1$, $D = 0.55$, $\kappa_+ = 2.1 \cdot \alpha'$, and $\kappa_- = -1.9 \cdot \alpha'$. (b) Front velocity amplification as a function of the nonreciprocal parameter α' close to pinning-depinning transitions, where the parameter of the left panel is $\alpha_c^- = [\alpha_c^{l-} = -0.250, \alpha_c^{r-} = -0.107]$ and of the right panel is $\alpha_c^+ = [\alpha_c^{l+} = 0.107, \alpha_c^{r+} = 0.250]$. The continuous curves correspond to fitting curves with a square root law of the form $v = v_0^+\sqrt{\alpha_c^+ - \alpha'}$ ($\alpha' > 0$) and $v = v_0^-\sqrt{|\alpha_c^-| + \alpha'}$ ($\alpha' < 0$), where the parameters of the left panel are $v_0^- = [v_0^{l-} = 3.093, v_0^{r-} = 3.184]$ and $\alpha_c^- = [\alpha_c^{l-} = -0.250, \alpha_c^{r-} = -0.107]$, and of the right panels are $v_0^+ = [v_0^{l+} = 3.183, v_0^{r+} = 3.084]$ and $\alpha_c^+ = [\alpha_c^{l+} = 0.107, \alpha_c^{r+} = 0.250]$.

equation [12,26] and limit of the extremely discrete system [7].

In the first approach, one can consider that the effective continuous equation for Eq. (4) takes the form [12,26]

$$\begin{aligned}\partial_t u(x,t) = {} & \eta + \mu u - a u^3 + D'[1 + \Gamma_{dx}(x)]\partial_{xx} u \\ & - v(1 + \kappa u^2)[1 + H_{dx}(x)]\partial_x u, \qquad (5)\end{aligned}$$

where $u(x,t)$ is the continuous variable for $u_i(t)$, which accounts for the average molecular reorientation around the critical angle θ_c, and D' and v account for diffusion and advective coupling that are poroportional to D and α, respectively. κ accounts for the nonlinear reciprocal coupling that is proportional to $\kappa_- + \kappa_+$. $\Gamma_{dx}(x)$ and $H_{dx}(x)$ are spatially periodic functions with a dx period, i.e., $\Gamma_{dx}(x + dx) = \Gamma_{dx}(x)$ and $H_{dx}(x + dx) = H_{dx}(x)$, where dx is the characteristic distance between the optical cells. These functions account for the discreteness effect of the bistable optical chain, which is associated with the Peierls-Nabarro potential [27]. In the continuum limit, which corresponds to strong coupling

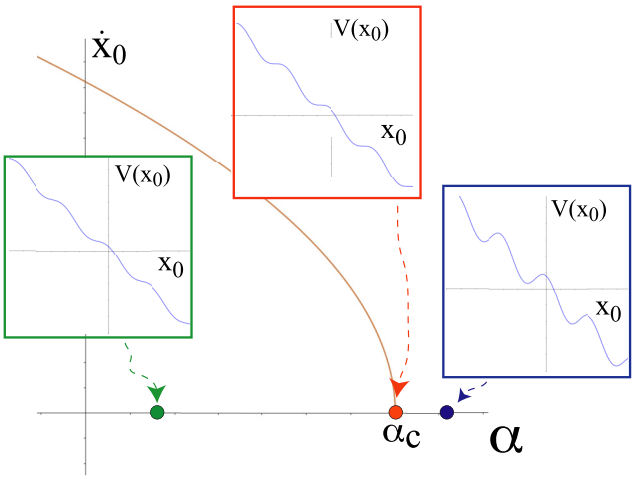

FIG. 6. Schematic representation of the front velocity as a function of the nonreciprocal parameter α'. Insets account for the potential $V(x_0)$ of Eq. (6) for different nonreciprocal parameter α' values.

between bistable cells, the system is described by Eq. (5), with Γ_{dx} and H_{dx} being small functions. Therefore, these functions can be considered as perturbative.

Ignoring the drift $v \ll 1$ in Eq. (5) and the discreteness effects, the system has front solutions $u_F(x - x_0(t))$ that connect stable states toward both flanks, where x_0 is a reference position from which the front dynamics are described. Note that $\dot{x}_0$ accounts for the front speed. The analytical expression for the front is typically unknown because determining this expression involves solving a nonlinear eigenvalue problem. The front velocity is only known in specific regions, such as around critical points like the Maxwell point [13] or near the bistability disappearance point [28]. By including the linear and nonlinear homogeneous drifts, fronts toward both flanks can present front speeds that must vanish around specific critical values of the nonreciprocal coupling α'_c. For example, if the front propagates against the direction of the drift, one naturally expects that there will be a point of absolute convective instability at which the front becomes motionless [29]. When fronts propagate in the same direction, the linear and nonlinear drift terms are responsible for absolute and convective instabilities. Likewise, discreteness effects are included close to this critical point (absolute-convective instability); the front's dynamics satisfy the Adler-like equation [30]:

$$\dot{x}_o = -\frac{dV}{dx_0} = \Delta_0(\alpha'_c - \alpha') + \gamma_{dx}(x_0), \tag{6}$$

where Δ_0 is a constant, the periodic function

$$\gamma_{dx}(x_0) \equiv \frac{\langle \partial_x u_F | [D' \Gamma_{dx}(x) \partial_{xx} u + H_{dx}(x) \partial_x u] \rangle}{\langle \partial_x u_F | \partial_x u_F \rangle}, \tag{7}$$

$\langle f(x)|g(x)\rangle = \int f(x)g(x)dx$ is an inner product, and $V(x_0)$ is a washboard potential (see Fig. 6). If the potential is an essentially decreasing (increasing) function with undulations, the front will propagate in a direction toward the right (left) flank (see Fig. 6). Changing the nonreciprocal parameter α', new maxima on the potential can emerge for a critical value of the parameter $\alpha' = \alpha'_c$, *pinning transition*. In the insets of Fig. 6, we illustrate the potential $V(x_0)$ for different nonreciprocal parameter α' values. Increasing the α' parameter even further, the potential clearly exhibits maxima and minima, which are responsible for the pinning phenomenon. Since the emergence of new maxima corresponds to a saddle-node bifurcation of the Adler-like equation, the dynamics around the transition is described by an equation of the form

$$\dot{x}_o = \Delta_0(\alpha'_c - \alpha') + \gamma_2 x_0^2, \tag{8}$$

where γ_2 is a constant. The solution of this equation has the form $x_o(t) = \sqrt{\Delta_0(\alpha'_c - \alpha')/\gamma_2}\tan[\sqrt{\Delta_0(\alpha'_c - \alpha')\gamma_2}(t - t_0)]$. Then, the time τ that the front takes to cross each zone with a unique maximum is $\tau = 1/\sqrt{\Delta_0(\alpha'_c - \alpha')\gamma_2}$ and the distance between these zones is dx. Hence, the average front speed is

$$\langle \dot{x}_o \rangle = dx\sqrt{\Delta_0(\alpha'_c - \alpha')\gamma_2}. \tag{9}$$

Hence, the average front velocity around the pinning-depinning point grows as the square root of the nonreciprocal parameter, which is consistent with the numerical observations of Eq. (9) and the experimental ones.

As mentioned, the pinning phenomenon and the square root law of front speed can be understood in the extremely discrete system, the second approach, using the strategy presented in Ref. [6]. Equation (4) becomes extremely discrete as $D \pm \alpha' \to 0$. At this limit, the front interface becomes extremely abrupt, formed by only three points, which we call u_{-1}, u_0, and u_1, where u_0 is the most central point. The dynamics of this central point satisfies

$$\begin{aligned}\partial_t u_0 = &-\frac{dU}{du_0} + (D + \alpha')(u_1 - u_0) + (D - \alpha')(u_{-1} - u_0) \\ &- (\kappa_+ u_1 - \kappa_- u_{-1})u_0^2,\end{aligned} \tag{10}$$

where $U(u_0) = -\eta u_0 - \mu u_0^2/2 + a u_0^4/4$. Note that the solutions $u_i(\eta, \mu, a, D, \alpha')$ are functions of the parameters. Assume that a critical point α'_c exists at which there is a transition from three solutions to one solution, saddle-node bifurcation of the above equation. Then, the following conditions must be satisfied:

$$\begin{aligned}&-\frac{dU}{du_0} + (D + \alpha'_c)(u_1 - u_0) + (D - \alpha'_c)(u_{-1} - u_0) \\ &\quad - (\kappa_+ u_1 - \kappa_- u_{-1})u_0^2 = 0, \\ &-\frac{d^2U}{d^2u_0} + 2D - 2(\kappa_+ u_1 - \kappa_- u_{-1})u_0 = 0.\end{aligned} \tag{11}$$

To study the dynamics of the front close to the saddle-node bifurcation, let us introduce the local variable $\varphi(t) \ll 1$ around the central position of the front $u_0 = u_0^c(\alpha_c) + \varphi(t)$. Using this ansatz in Eq. (10), expanding in the Taylor series, and using the above relations, after straightforward calculations, one obtains the equation

$$\partial_t \varphi = \Gamma_0(\alpha' - \alpha_c) + \Gamma_2 \varphi^2, \tag{12}$$

where $\Gamma_0 \equiv u_0^c + u_1^c - u_{-1}^c$ and $\Gamma_2 \equiv -6u_0^c$; indeed, one recovers Eq. (8). Therefore, the average front speed follows a square root as a function of the nonreciprocal parameter.

In conclusion, coupled bistable one-dimensional systems exhibit nonlinear waves that propagate to minimize one state over another. However, due to the discreteness of these systems, nonlinear states become motionless when changing the parameters, and a failure propagation phenomenon occurs, even though one state is more stable than another. We have shown that nonreciprocal couplings can also induce this phenomenon. Our findings have the potential to reveal new methodologies for the manipulation of nonlinear waves in magnetic chains [31], the coupling of lasers [32,33], thermal spin photonics coupling slabs [34], the release of calcium waves in living cells [5], coupled chemical reactors [35], the arrays of coupled diode resonators [36], the chains of paramagnetic colloidal particles [37], the covalent chemical reactions on single-walled carbon nanotubes [38], and the dynamics of neuron chains [39].

Unexpectedly, one can find regions where propagation cannot occur on any flank. In this region, one expects to observe stable localized states. Studies in this direction are in progress. Likewise, the extension of this phenomenon to more dimensions and different geometries opens exciting questions about how these nonlinear waves propagate and what effects the nonreciprocal terms can have on these dynamics.

Acknowledgments. The authors acknowledge the financial support of FONDECYT Project No. 1210353 and ANID Millenium Science Initiative Program-ICN17_012, Chile (MIRO). M.G.C. acknowledges support from CMM through ANID PIA Grant No. AFB17000.

Data availability. The data that support the findings of this article are not publicly available. The data are available from the authors upon reasonable request.

[1] J. P. Keener, Propagation and its failure in coupled systems of discrete excitable cells, SIAM J. Appl. Math. **47**, 556 (1987).
[2] J. P. Keener and J. Sneyd, *Mathematical Physiology* (Springer, New York, 1998), Chap. 9.
[3] J. P. Laplante and T. Erneux, Propagation failure and multiple steady states in an array of diffusion coupled flow reactors, Physica A **188**, 89 (1992).
[4] J. Keizer, G. D. Smith, S. Ponce Dawson, and J. E. Pearson, Saltatory propagation of Ca^{2+} waves by Ca^{2+} sparks, Biophys. J. **75**, 595 (1998).
[5] S. P. Dawson, J. Keizer, and J. E. Pearson, Fire–diffuse–fire model of dynamics of intracellular calcium waves, Proc. Natl. Acad. Sci. USA **96**, 6060 (1999).
[6] A. Carpio and L. L. Bonilla, Wave front depinning transition in discrete one-dimensional reaction-diffusion systems, Phys. Rev. Lett. **86**, 6034 (2001)
[7] A. Carpio, L. L. Bonilla, A. Wacker, and E. Schöll, Wave fronts may move upstream in semiconductor superlattices, Phys. Rev. E **61**, 4866 (2000).
[8] V. M. Karpan, Y. Zolotaryuk, P. L. Christiansen, and A. V. Zolotaryuk, Discrete kink dynamics in hydrogen-bonded chains: The one-component model, Phys. Rev. E **66**, 066603 (2002).
[9] C. J. Efthimiou and M. D. Johnson, Domino waves, SIAM Rev. **49**, 111 (2007)
[10] Y. Ishimori and T. Munakata, Kink dynamics in the discrete sine–Gordon system a perturbational approach, J. Phys. Soc. Jpn. **51**, 3367 (1982).
[11] M. Peyrard and M. D. Kruskal, Kink dynamics in the highly discrete sine–Gordon system, Physica D **14**, 88 (1984)
[12] M. G. Clerc, R. G. Elías, and R. G. Rojas, Continuous description of lattice discreteness effects in front propagation, Philos. Trans. R. Soc. A **369**, 412 (2011).
[13] Y. Pomeau, Front motion, metastability and subcritical bifurcations in hydrodynamics, Physica D **23**, 3 (1986).
[14] L. V. Alekseeva, I. V. Povkh, V. I. Stroganov, B. I. Kidyarov, and P. G. Pasko, A nonreciprocal optical element, J. Opt. Technol. **70**, 525 (2003).
[15] I. M. Mirza, W. Ge, and H. Jing, Optical nonreciprocity and slow light in coupled spinning optomechanical resonators, Opt. Express **27**, 25515 (2019).
[16] P. Yang, X. Xia, H. He, S. Li, X. Han, P. Zhang, G. Li, P. Zhang, J. Xu, Y. Yang, and T. Zhang, Realization of nonlinear optical nonreciprocity on a few photon level based on atoms strongly coupled to an asymmetric cavity, Phys. Rev. Lett. **123**, 233604 (2019).
[17] R. Fleury, D. L. Sounas, C. F. Sieck, M. R. Haberman, and A. Alù, Sound isolation and giant linear nonreciprocity in a compact acoustic circulator, Science **343**, 516 (2014).
[18] H. Lira, Z. Yu, S. Fan, and M. Lipson, Electrically driven nonreciprocity induced by interband photonic transition on a silicon chip, Phys. Rev. Lett. **109**, 033901 (2012).
[19] Z. Wang, Y. Chong, J. D. Joannopoulos, and M. Soljacic, Observation of unidirectional backscattering-immune topological electromagnetic states, Nature (London) **461**, 772 (2009).
[20] D. L. Sounas, C. Caloz, and A. Alù, Giant non-reciprocity at the subwavelength scale using angular momentum-biased metamaterials, Nat. Commun. **4**, 2407 (2013).
[21] C. Coulais, D. Sounas, and A. Alù, Static non-reciprocity in mechanical metamaterials, Nature (London) **542**, 461 (2017).
[22] P. J. Aguilera-Rojas, K. Alfaro-Bittner, M. G. Clerc, M. Díaz-Zúñiga, A. Moya, D. Pinto-Ramos, and R. G. Rojas, Nonlinear wave propagation in a bistable optical chain with nonreciprocal coupling, Commun. Phys. **7**, 195 (2024).
[23] M. G. Clerc, S. Residori, and C. Riera, First-order Freedericksz transition in the presence of a light driven feedback, Phys. Rev. E **63**, 060701 (2001).
[24] S. Residori, Patterns, fronts, and structures in a liquid crystal light valve with optical feedback, Phys. Rep. **416**, 201 (2005).
[25] See Supplemental Material at https://link.aps.org/supplemental/10.1103/9ypt-4kvs for the relationship between the parameters of Eqs. (2) and (4).
[26] K. Alfaro-Bittner, M. G. Clerc, M. A. Garcia-Nustes, and R. G. Rojas, π-kink propagation in the damped Frenkel-Kontorova model, Europhys. Lett. **119**, 40003 (2017).
[27] F. R. N. Nabarro, *Theory of Crystal Dislocations* (Dover, New York, 1987).

[28] P. J. Aguilera-Rojas, K. Alfaro-Bittner, M. G. Clerc, G. González-Cortés, and R. G. Rojas, The universal law of the front speed close to the disappearance of bistability, Chaos Solitons Fract. **169**, 113241 (2023).

[29] L. P. Pitaevskii and E. M. Lifshitz, *Physical Kinetics* (Butterworth-Heinemann, Oxford, 2012), Vol. 10.

[30] R. Adler, A study of locking phenomena in oscillators, Proc. IRE **34**, 351 (1946).

[31] T. J. Sato and K. Matan, Nonreciprocal magnons in noncentrosymmetric magnets, J. Phys. Soc. Jpn. **88**, 081007 (2019).

[32] Y. Jiang, S. Maayani, T. Carmon, F. Nori, and H. Jing, Nonreciprocal phonon laser, Phys. Rev. Appl. **10**, 064037 (2018).

[33] H. Shimizu, Y. Kono, S. Goto, and T. Mori, Demonstration of a magnetically controllable Fabry-Perot laser and an unidirectional ring laser utilizing a nonreciprocal semiconductor optical amplifier, Appl. Phys. Express **4**, 022201 (2011).

[34] C. Khandekar and Z. Jacob, Thermal spin photonics in the near-field of nonreciprocal media, New J. Phys. **21**, 103030 (2019).

[35] J. P. Laplante and T. Erneux, Propagation failure in arrays of coupled bistable chemical reactors, J. Phys. Chem. **96**, 4931 (1992).

[36] M. Löcher, D. Cigna, and E. R. Hunt, Noise sustained propagation of a signal in coupled bistable electronic elements, Phys. Rev. Lett. **80**, 5212 (1998)

[37] F. Martinez-Pedrero, P. Tierno, T. H. Johansen, and A. V. Straube, Regulating wave front dynamics from the strongly discrete to the continuum limit in magnetically driven colloidal systems, Sci. Rep. **6**, 19932 (2016)

[38] S. Deng, Y. Zhang, A. H. Brozena, M. L. Mayes, P. Banerjee, W.-A. Chiou, G. W. Rubloff, G. C. Schatz, and Y. Wang, Confined propagation of covalent chemical reactions on single-walled carbon nanotubes, Nat. Commun. **2**, 382 (2011).

[39] D. McLaughlin, R. Shapley, M. Shelley, and D. J. Wielaard, A neuronal network model of macaque primary visual cortex (V_1): Orientation selectivity and dynamics in the input layer 4Cα, Proc. Natl. Acad. Sci. USA **97**, 8087 (2000).